

Function Graded Carbon Micro-Structures for Powerless Photon Sensing with Intriguing μm -Scale Position Sensitivity

Amin Karamati, Wangda Qu, Xianglan Bai, and Xinwei Wang*

Partial laser treatment is introduced to carbon-based microfibers to generate excellent photon sensing capability without bias. This treatment brings about a Seebeck coefficient distribution along the sample's length, out of which a photovoltage with no external bias is generated and sensed. Using a line-shaped laser spot, carbon microfiber (CMF), graphene microfiber (GMF), and graphene aerogel fiber (GAF) are investigated for their response to μm -scale photon irradiation. A higher sensitivity for the incident photon is found for the GAF with no position sensitivity. More Seebeck coefficient variation is also observed for the GAF considering the amount of laser power used for the laser treatment. A weaker Seebeck coefficient spatial variation is observed for the GMF compared with the GAF. However, its photovoltage shows an abrupt magnitude change from the laser-treated region to the non-treated one. Despite the low spatial variation of the Seebeck coefficient for the CMF, it features an excellent and accurate position-sensitive photoresponse with polarization change over a distance of $\approx 100 \mu\text{m}$. Such unique capability prompts novel applications in using partially annealed CMF for sensing the position of optical beams at the microscale.

been identified as the origins of their photoresponse: the photovoltaic effect and the photo thermoelectric (PTE) effect.^[5] In the photovoltaic effect, as the incident photons create electron-hole pairs, a forced separation between the electrons and holes in the presence of an existing electric field generates a photocurrent.^[6] Carbon-based materials have been explored for their potential applications in photovoltaics, where their high surface area, good conductivity, and optical transparency make them promising candidates for photoconversion.^[7–9] In addition, the temperature difference created at different areas of the component as a result of photon energy absorption is known as the photo thermoelectric effect. This temperature difference is subsequently turned into an output voltage by the Seebeck effect.^[10–13]

Xu et al. reported a surprising photovoltage during optical irradiation of suspended aligned carbon nanotube (CNT) bundles with neither bias voltage nor temperature

difference from one end to the other.^[5] They showed that this photo response is mainly related to the Seebeck coefficient rather than being a photovoltaic process. Under the irradiating power of 91 mW, where only a very small amount shining on the sample, a $\approx 120 \mu\text{V}$ photovoltage was generated. They also discovered a nonuniform local Seebeck coefficient along the bundle using localized heating and scanning.^[5] A linear decrease in the Seebeck coefficient from $7 \mu\text{V K}^{-1}$ to $-7.5 \mu\text{V K}^{-1}$ was reported for the root to the tip of the CNT bundles. Xiong et al.^[14] coated a reduced graphene oxide (rGO) film on a polydimethylsiloxane (PDMS) layer to create an effective photothermal film. This detector was able to detect laser emissions of 6.37 kW m^{-2} at 473, 532, and 808 nm with the corresponding responsivities of 15.6, 14.6, and 19.4 V W^{-1} . PEDOT: PSS/graphene composite mid-infrared photodetectors as the self-powered ones working based on the photo-thermoelectric effect were investigated by Zhang et al.^[15] The highest photo detectivity of $1.4 \times 10^7 \text{ cm Hz}^{0.5} \text{ W}^{-1}$ was reported for 3 wt.% of graphene loading on PEDOT: PSS. Wang et al.^[16] proposed a device architecture based on graphene to enhance its photo response. A set of split gates was used to create a p-n junction in graphene to increase the PTE current generation. A gap plasmon structure was used to absorb the majority of the incident light to trigger localized heating. Based on their

1. Introduction

Carbon-based materials have been widely investigated in recent years for their potential in optoelectronic applications, particularly to generate photocurrent.^[1–4] Two main mechanisms have

A. Karamati, X. Bai, X. Wang
Department of Mechanical Engineering
271 Applied Science Complex II
Iowa State University
Ames, IA 50011, USA
E-mail: xwang3@iastate.edu

W. Qu
Laboratory of Lignin-based Materials
College of Life Sciences
Qingdao Agricultural University
Qingdao 266109, P. R. China

 The ORCID identification number(s) for the author(s) of this article can be found under <https://doi.org/10.1002/adom.202301377>

© 2023 The Authors. Advanced Optical Materials published by Wiley-VCH GmbH. This is an open access article under the terms of the Creative Commons Attribution License, which permits use, distribution and reproduction in any medium, provided the original work is properly cited.

DOI: 10.1002/adom.202301377

experiments, the generated photocurrent was 25 times greater than the unenhanced case. A suspended PTE detector based on the SWCNT/PEDOT:PSS composite was characterized by Wang et al.^[17] They attributed the obtained stable photoresponse to the strong π - π interaction between SWCNTs and PEDOT: PSS. Without bias, a peak detectivity of $1.9 \times 10^7 \text{ cm Hz}^{0.5} \text{ W}^{-1}$ was acquired. St-Antoine et al.^[18] investigated the local photovoltage properties of suspended SWNT sheets. They reported photovoltage amplitudes up to 0.36 mV using a 1.2 mW laser irradiating the film. Additionally, they also showed that the photovoltage has a strong position-dependent effect. Based on their findings, the photoresponse maximum was toward the film center and away from the contact, and the photothermoelectric effect was the source of the photovoltage in the suspended films.

For carbon structures, most of the photon sensing capability is due to the photon-thermal-electrical effect: the photon is absorbed to increase the temperature, and the temperature change will cause electrical resistance change. This resistance change is measured to probe the photon irradiation. This resistance change that can be observed as the voltage change is like the Transient Photo-Electro-Thermal (TPET) technique. In this technique, which will be discussed in more detail in the later sections, a typical sample's transient behavior is probed when irradiated by a laser (photon) source.

In this work, we utilize a laser to induce permanent local structure change and nonuniformity in carbon microfiber (CMF), graphene microfiber (GMF), and graphene aerogel fiber (GAF), which leads to a nonuniform Seebeck coefficient through the structure. Subsequently, this structure is used to sense photons via the generated photovoltage without power input. We will show this photon sensing capability features extreme position sensitivity in CMFs, which is very unique and novel.

2. Carbon Microfiber: Structure Grading and Photon Sensing

Photon sensing technique, which is similar to the TPET, is used to probe the photovoltage response of the microscale samples in this work. In this technique, a micro/nanoscale sample is suspended between two electrodes. Silver paste is applied to the ends of the sample to make the connection electrically and thermally secure. Then, a step-modulated continuous wave (CW) laser irradiates the sample locally. Subsequently, the sample's resistance changes as its temperature rises, causing a transient shift in voltage through the sample. In order to measure the voltage change during the TPET, a small DC current is also passed through the sample. However, in the photon sensing technique, no DC current is applied to the sample. The schematic of this technique is shown in **Figure 1c**. The transient electrothermal (TET) technique is also used in this study. In this technique developed in our lab in 2007,^[19] rather than a step laser, a step DC current is passed through the micro/nanoscale sample. Due to Joule heating, the resistance of the sample changes transiently until the temperature reaches a steady state. This transient behavior is obtained and analyzed to determine the thermal diffusivity of the sample. It is reasonable to assume that the heat conduction is one-dimensional along the sample, given the high length-to-thickness ratio of the microfibers. The equation below gov-

erns the 1D transient heat conduction through the microfiber (x) as^[19]:

$$\frac{\partial(T\rho c_p)}{\partial t} = \frac{\partial}{\partial x} \left(k \frac{\partial T}{\partial x} \right) + \dot{q} \quad (1)$$

where ρ , c_p , and k are the sample's density, specific heat, and thermal conductivity, respectively. Temperature is denoted as T , and \dot{q} in W m^{-3} is the heating generated by the electrical current.

The average dimensionless temperature rise of the sample can then be derived by solving Equation 1 as^[19]:

$$T^* = \frac{96}{\pi^4} \sum_{m=1}^{\infty} \frac{1 - \exp[-(2m-1)^2 \pi^2 \alpha t / L^2]}{(2m-1)^4} \quad (2)$$

where α is the thermal diffusivity, and L is the sample length. Here we will use TET for two purposes. First, we will compare the characteristics time (t_c) of the TET signal to that of the photovoltage signals under step laser heating. Second, the TET will be used to measure the thermal diffusivity of the microfibers from which the thermal conductivity of them can be determined. The thermal conductivity is needed for the calculation of the local Seebeck coefficient for the microfibers in Equation 3. It is worth noting that the characteristic time is defined as the time when T^* reaches 0.8665.^[19]

First, a CMF is held on a piece of glass to induce a permanent change in the structure. Half of the sample is then irradiated (annealed) by a CW 532 nm laser (DPSS Inc.) with a power of $\approx 2.0 \text{ W}$ for 200 s (**Figure 1a**) while the sample is in a vacuum chamber ($< 3 \text{ mTorr}$). A blade is used to shield the other half of the sample from irradiation. The laser spot size is measured to be 2 mm. **Figure 1b,d** shows the suspended half-treated CMF and its schematic on a trench with a length of 2.087 mm and diameter of 51.6 μm . For making the substrate, a glass slide with 1 mm thickness is cut into two parts. Then, both parts are attached to another full glass slide with a clearance of $\approx 2 \text{ mm}$ to make the trench. In this way, a trench with $\approx 2 \text{ mm}$ width and 1 mm depth is created. The microfiber is transferred to the trench via a tweezer. The CMF investigated in this work is made using pyrolytic lignin (PL), and detailed information about the sample synthesis may be found in the work by Qu et al.^[20] Briefly, a twin-screw microcompounder is used to extrude $\approx 6 \text{ g}$ of pyrolytic lignin at temperatures between 115 and 120 $^\circ\text{C}$. At speeds of up to 100 m min^{-1} , the fibers are coiled onto a roller. In a muffle furnace, the spun fibers are heated to 280 $^\circ\text{C}$ at a rate of 0.3 $^\circ\text{C min}^{-1}$, kept for 1 h, and then subjected to oxidative stabilization. In an argon-filled tube furnace, carbonization is carried out. The stabilized fibers are then heated for 1 h at a rate of 3 $^\circ\text{C min}^{-1}$ up to 1000 $^\circ\text{C}$. To irradiate the sample to check its photoresponse, the laser beam is reshaped to a line-shape of 0.1 mm in width and 5.5 mm in length. The TET signal of the sample, along with the photovoltage signal of the sample under laser (photon) irradiation, are given in **Figure 1e**. The t_c of the TET and the photovoltage signals (e.g., $x = 0.2 \text{ mm}$) are calculated to be 0.788 s and 0.578 s. The similar timescale for the TET and photon sensing firmly proves the thermal origin of the obtained photovoltage.

Figure 2a depicts the obtained transient photovoltage for different locations of the laser irradiation on CMF with no external bias. Note the contact between the laser treated part and the

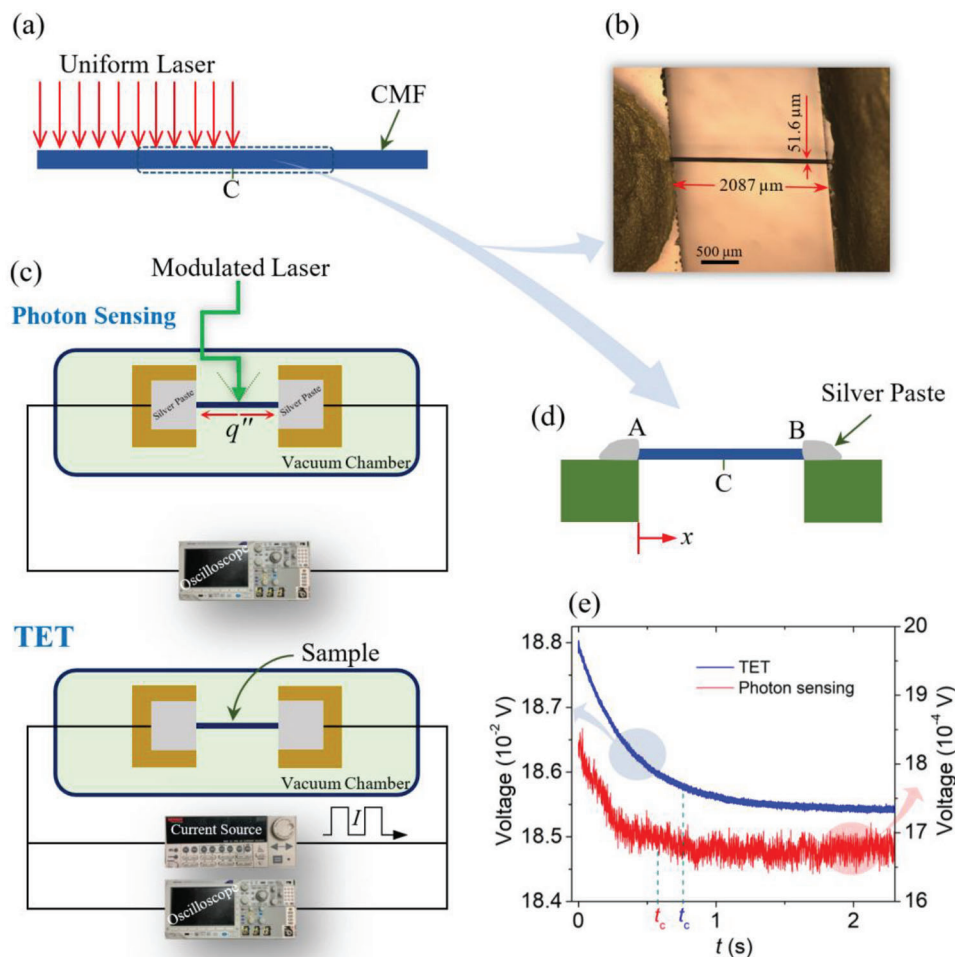


Figure 1. a) The schematic of the laser treatment on half of the microfiber (e.g., CMF). b) Optical image of the suspended carbon microfiber of 2.087 mm length. c) Schematics of the TPET and TET techniques. d) Schematic of the suspended laser-treated microfiber: half of the sample is laser-treated, and the other half is not. e) The TET and the photovoltage signals for an arbitrary location ($x = 0.2$ mm) of the CMF to compare their characteristic times.

electrode is taken as the “+” side during our voltage measurement. This is followed for other samples as well. The “On” and “Off” periods of the incident laser beam for the annealed (laser-treated) and unannealed (not-treated) locations of the CMF are shown in this figure. A laser power range of 150–220 mW is then used to irradiate the sample. As a result, a photovoltage between ≈ 0.06 mV and ≈ 0.18 mV is obtained from the CMF. The most important observation from this figure is that when the laser irradiates the laser-treated and non-treated regions, the voltage signs are opposite to each other, indicating that the sensor (i.e., the CMF) is very sensitive to the position of the laser (photon). This firmly confirms the position sensitivity of the sensor.

Since different laser powers are used to stimulate the sample in different locations, ΔV_{PV} is defined as the photovoltage normalized to the lowest laser power (150 mW) used for obtaining the photovoltage signal from the sample. Figure 2b shows the ΔV_{PV} variation with the location. It ranges between -247 μ V and $+179$ μ V from the annealed to unannealed regions. The characteristic time is also evaluated for different laser locations shown in Figure 2b. The t_c of various locations of the sample are quite different, with a sharp shift in the boundary between the laser-

treated and non-treated regions. The difference between the characteristic times of different locations can be attributed to the variation in the structure and thermal properties (e.g., k , ρc_p , and θ_T : temperature coefficient of resistivity) through the CMF’s length. However, their similar t_c (≈ 0.1 – 0.5 s) order indicates that the photovoltage for different locations arises from the thermal response of the CMF.

We showed that the photovoltage stems from the thermoelectric effect. So, the Seebeck coefficient (S) should vary along the sample; otherwise, there would be no photovoltage out of the thermoelectric effect.^[5] The local Seebeck coefficient can be calculated as^[5]:

$$S_x = \frac{dV_{PV}}{dx} / \left(\frac{Q_{abs}}{Ak} \right) \quad (3)$$

where Q_{abs} is the portion of the laser energy absorbed by the sample, A is the sample’s cross-sectional area, and k is the thermal conductivity. The absorbed energy by the sample can be calculated as $Q_{abs} = (D/L) \cdot Q_{Laser}$, where D is the microfiber’s diameter, L is the length of the line-shaped laser beam, and Q_{Laser} is the

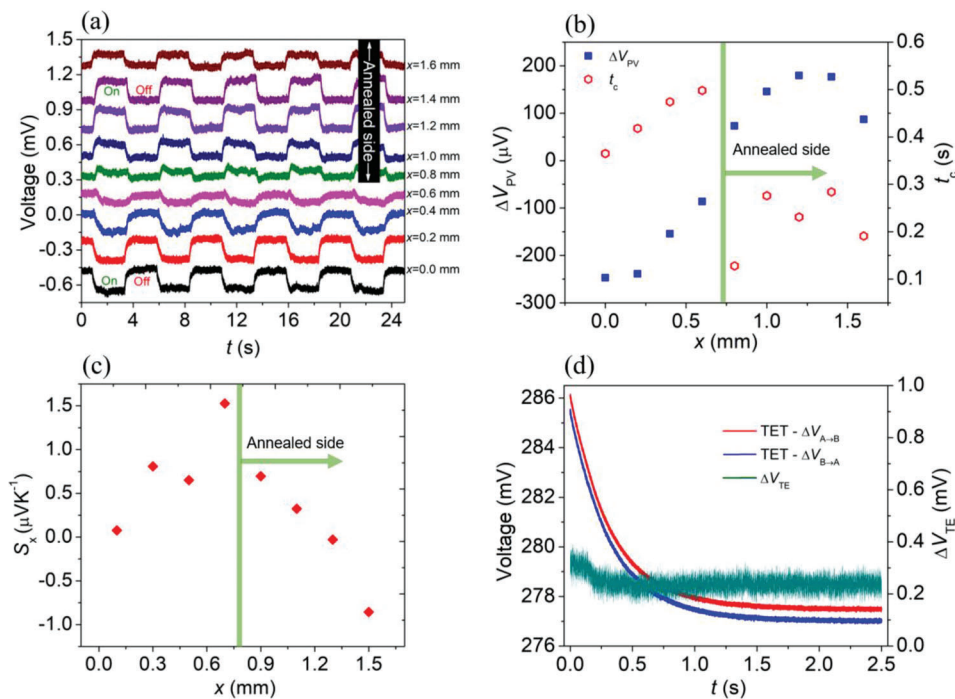


Figure 2. a) Demonstration of the CMF's photovoltage change with time upon step laser (photon) irradiation for different locations on the sample. The "On" and "Off" periods of the incident laser beam are shown for one step for $x = 0$ mm and $x = 1.4$ mm, for instance. b) Photovoltage variation for different locations of the CMF, which is normalized based on the lowest laser power (150 mW) used for obtaining the photoresponse. Also shown in this figure is the characteristic time of the photoresponse for the CMF with the location. c) Local Seebeck coefficient variation of the CMF with the location. d) The bi-directional TET (voltage) signals (i.e., $\Delta V_{A \rightarrow B}$ and $\Delta V_{B \rightarrow A}$) for the CMF along with the embedded TE signal, which is calculated as $\Delta V_{TE} = (\Delta V_{A \rightarrow B} - \Delta V_{B \rightarrow A})/2$.

laser power used. The k value is calculated as $k = \rho c_p \alpha_{eff}$, where ρc_p of graphite (1.552×10^6 J m $^{-3}$ K $^{-1}$) is used for the CF and α_{eff} is the effective thermal diffusivity measured to be 1.16×10^{-6} m 2 s $^{-1}$ using the TET technique. So, k of the CMF is found to be 2.48 W m $^{-1}$ K $^{-1}$. The variation of S_x with location is presented in Figure 2c. It ranges between -0.85 μ V K $^{-1}$ and $+1.52$ μ V K $^{-1}$. In fact, this variation in S_x brings about the photovoltage sign change shown in Figure 2b. Although the values of S_x and its variation seem to be small; however, the position sensitivity with the laser spot location shown in Figure 2a is significantly high.

To further verify that the induced photovoltage is caused by the thermal effect, the TET method is utilized here. This thermal effect (if it exists) should show up as the thermoelectric (TE) voltage combined with the TET signal that is based on the Joule heating of the sample.^[5] However, this hypothetical TE effect is embedded in the TET signal, and for its determination, two different TET tests in terms of the current direction should be conducted. If the sample's left and right ends are called A and B, respectively, $\Delta V_{A \rightarrow B}$ is the TET voltage for the case that the step current flows from the edge point of A to B. For the TET tests, a step current of 2 mA with a frequency of 0.2 Hz is used. The corresponding TET signals are shown in Figure 2d. During the TET measurement, the observed voltage change consists of two effects. The first one is induced due to the resistance change, and the other one is the TE effect. The first term is dependent on the direction of the current used in the TET. However, as mentioned earlier, the TE voltage is direction-independent. It should be noted that the

absolute value of TE voltage remains constant for either current direction. So, based on these explanations, we can express the total TET voltage signal as $\Delta V_{TET(A \rightarrow B)} = \Delta R \cdot I_0|_{AB} + \Delta V_{TE}$ and $\Delta V_{TET(B \rightarrow A)} = \Delta R \cdot I_0|_{BA} - \Delta V_{TE}$, when the current is from A to B and vice versa, respectively. To extract the TE effect from these bi-directional TETs, the TE voltage can be calculated as $\Delta V_{TE} = (\Delta V_{A \rightarrow B} - \Delta V_{B \rightarrow A})/2$. Based on Figure 2d, a ΔV_{TE} of 84.3 μ V is obtained from a TET voltage change of 8.64 mV. The t_c for this TE voltage is calculated to be 0.276 s, similar in scale to the t_c of the photon-sensing photovoltages, hence confirming the thermal origin for the photovoltages of the CMF. It is worth mentioning this effect can also be used for thermal sensing if a connected CMF is placed in a hot/cold environment and a temperature gradient is established in it.

Raman scanning is also conducted for the CMF to probe the structural change of the sample that has come about due to half laser annealing treatment. The sp 2 ring-breathing mode, typical of graphene-like materials, is indicated by the Raman D-band, which corresponds to the A $_{1g}$ phonon mode. The E $_{2g}$ in-plane vibrational mode relates to the Raman G-band. Figure 3a shows two prominent D (1354 cm $^{-1}$) and G (1589 cm $^{-1}$) peaks as the characteristic of carbon-based materials that are present in the Raman spectra.^[21,22] The normalized ratio of I_D/I_G is also used to assess the defect density of the sample. The intensity variation of D and G peaks (i.e., I_D and I_G) as well as their ratio (I_D/I_G), are shown in Figure 3b. Based on these results, no specific variation is seen in the structure through the CMF's length, and they

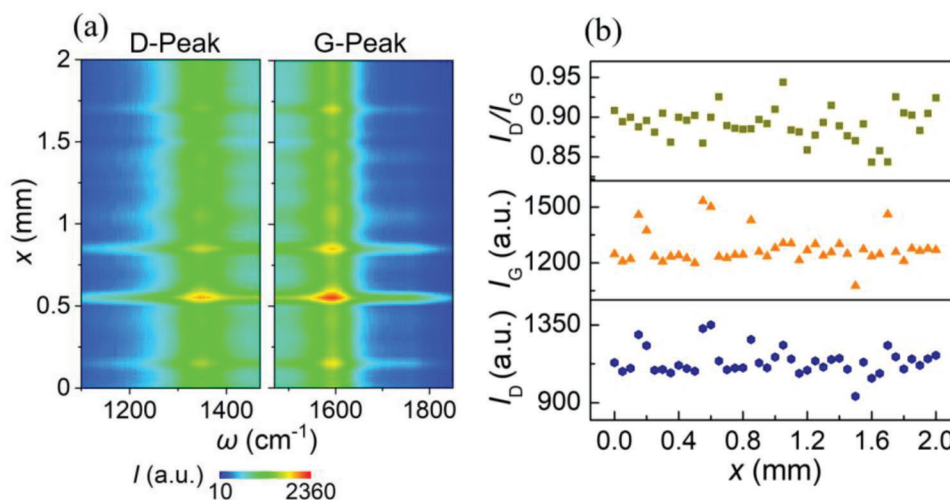


Figure 3. a) Contour map for D and G peaks versus Raman wavenumber and location for the CMF. b) The D peak to G peak intensities (i.e., I_D and I_G) and their ratio (I_D/I_G) variation for the half laser-treated CMF to show the structure variation along the sample.

remain quite consistent. The I_D/I_G is in a range of 0.85–0.95 through the sample's length, showing a good quality for the CMF used in this work compared to the value of 2.53 reported by Qu et al.^[21]

The results of similar investigations will be discussed in the next sections for GMF and GAF samples. In short, our Raman spectroscopy study shows the laser treatment on half of the CMF makes little change in its structure. However, this treatment dramatically changes the Seebeck coefficient, leading to an intriguing and precise position-sensitive photoresponse of the microfiber.

3. Microfibers Composed of Graphene: Photon Sensing

3.1. Photon Sensing by Graded Graphene Microfibers (GMFs)

In this section, we apply the laser treatment mentioned above on GMFs. In this study, we synthesize graphene microfibers by using a hydrothermal procedure.^[23] To create the aqueous suspension of graphene oxide (GO), enough amount of 30 mg ml⁻¹ GO and DI water are mixed. The suspension is next put in an ultrasonic bath for one hour to create a homogenous suspension. The suspension is then injected into a 10 cm long glass tube with an inner diameter of 1.0 mm. The pipes are sealed at both ends before being baked for 2 h at 230 °C. Finally, high-quality GMFs with a diameter of 88.6 μm are formed after extracting from the pipes. After conducting the laser annealing treatment on nearly half of the GMF with a laser power of ≈2.0 W and beam diameter of 2 mm for 200 s under vacuum condition (< 3 mTorr), it is suspended on a trench.

The suspended sample is shown as the inset in **Figure 4h** after applying the silver paste on its ends. The length of the sample is measured to be 1.929 mm. The linear I - V curve for the GMF is shown in **Figure 4c** indicating a good-quality contact with ohmic behavior. The little nonlinear behavior at the left side ($-0.8 \sim -0.4$ V) is far beyond the testing range in our work. The range of laser power used for obtaining the photovoltage response of

the sample is 17.5–120 mW. The width and the length of the line-shaped laser beam are 0.1 mm and 5.5 mm, respectively. As illustrated in **Figure 4a,b**, different levels of photovoltages are observed at different step laser (photon) irradiation locations using the laser with a wavelength of 532 nm and 405 nm, respectively. The step laser irradiation on the sample is indicated by “On” and “Off” marks in **Figure 4a,b** for one step, and it continues for the further time. Moreover, no considerable change in the photoresponse of the GMF is observed comparing the results by using the 532 nm and 405 nm lasers. However, one important point is that, unlike the CMF, it does not change sign through the length of the sample. Our below analysis will focus on the results using the 532 nm laser. This observation is also clearly shown in **Figure 4d**, where different laser locations' ΔV_{PV} are provided. Besides, the ΔV_{PV} is the normalized photovoltage based on the lowest laser power (i.e., 17.5 mW). Based on these data, the photosensitivity becomes higher moving from $x = 0.1$ mm to $x = 0.8$ mm, jumping back to lower sensitivity from $x = 0.9$ mm to the other end of the sample at $x = 1.8$ mm. As far as the t_c is concerned, there is an overall decreasing trend from the laser-treated to not-treated locations from 0.5 s to 0.3 s. Like the CMF, this slight difference can be related to the thermal properties' variation (e.g., thermal conductivity and specific heat) through the GMF's structure. The TET testing is also conducted on the GMF, and the t_c is found to be 0.33 s. The similar characteristic time for the photovoltage and the TET signal confirms the thermal effect origin of the GMF's photoresponse. The S_x for the GMF is calculated based on Equation 3. The α_{off} of the GMF is measured to be 2.32×10^{-6} m² s⁻¹ via TET, and its k is calculated to be 3.6 W m⁻¹ K⁻¹ considering the ρ_{cp} to be 1.552×10^6 J m⁻³ K⁻¹, the same as graphite. Despite the photovoltage and ΔV_{PV} that do not change the sign through the sample, S_x changes the sign from the laser-treated to not-treated regions (**Figure 4e**). The Seebeck coefficient values for the GMF are much higher than that of CMF, ranging from -54.8 μV K⁻¹ to $+121.5$ μV K⁻¹. This makes the GMF more sensitive to the incoming photons. This higher sensitivity can be realized by comparing the laser powers (mentioned earlier) used to stimulate the samples.

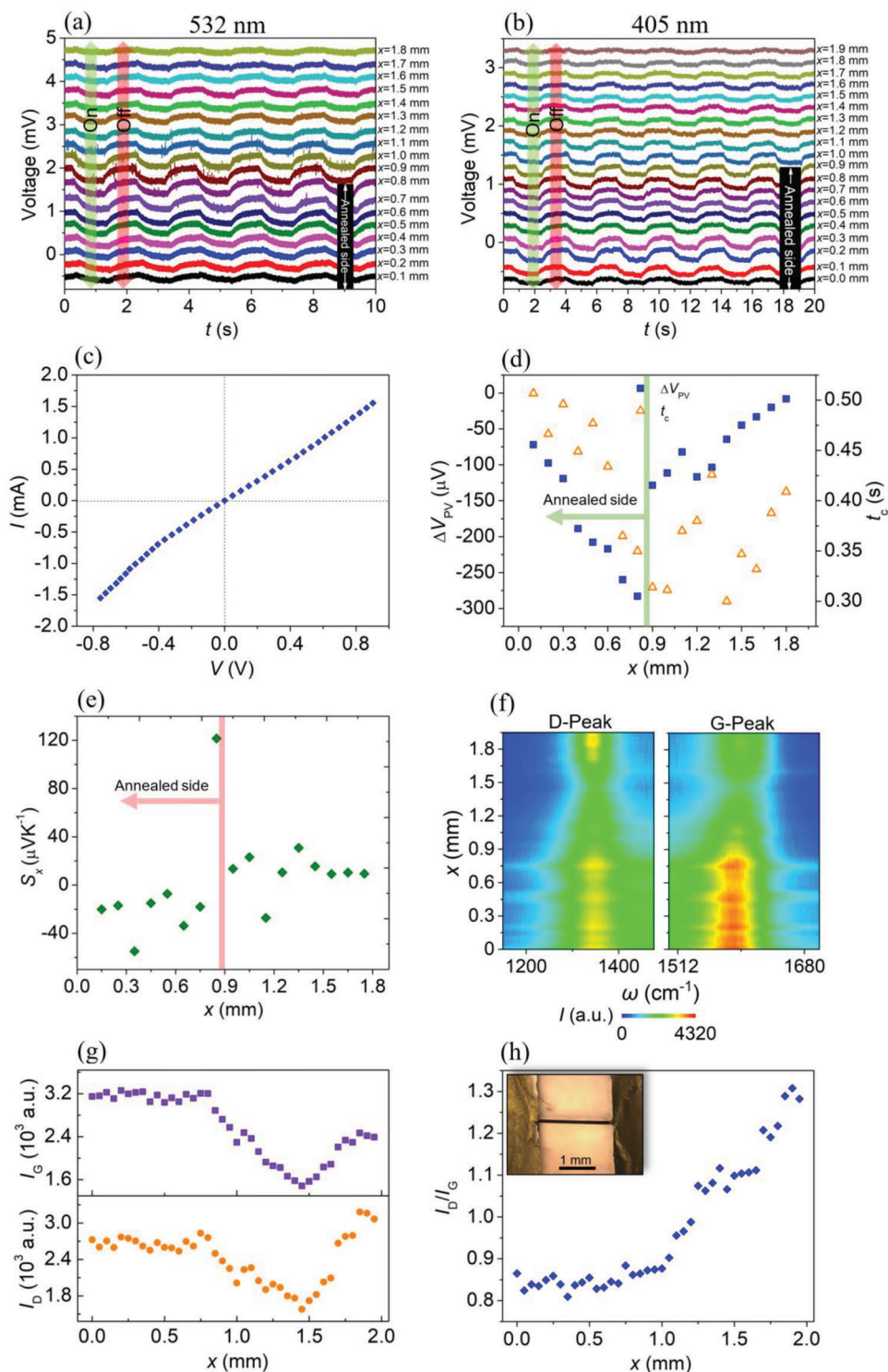


Figure 4. The GMF's photovoltage changes with time under step laser irradiation for different locations of the sample using the laser with a wavelength of a) 532 nm and b) 405 nm. The "On" and "Off" status of the incident laser beam are also shown for one period on both graphs. c) I - V (current vs voltage) curve for the GMF to show the quality of the sample's contact with the silver paste. d) Photovoltage variation for different locations of the GMF based on the lowest laser power (17.5 mW) used for obtaining the photoresponse. The characteristic time of the photoresponse for the GMF with location is also given. e) Local Seebeck coefficient variation of the GMF with the location. f) Contour map for D and G peaks versus Raman wavenumber and location for the GMF. g) The D peak to G peak intensities (i.e., I_D and I_G) and h) their ratio (I_D/I_G) variation for the half laser-treated GMF to show the structure variation along the sample. The inset is the optical image of the suspended GMF with 1.929 mm length.

The Raman scanning for the GMF identifies two main peaks of D at round 1351 cm^{-1} and G at $\approx 1590\text{ cm}^{-1}$ for different locations (Figure 4f) with clear enhancement in G peak intensity for the laser-treated locations. 2D peak is not identified for the GMF, even using higher laser powers. The corresponding variation of the D and G peaks' intensities is shown in Figure 4g. Figure 4h clearly shows structure improvement for the laser-treated region (i.e., $x = 0.0\text{ mm}$ to $x = 0.8\text{ mm}$). The I_D/I_G is lower for the laser-annealed regions (< 0.9), after which it starts rising to higher values to nearly 1.3. As mentioned earlier, GO is the typical precursor substance used to synthesize graphene fibers and other graphene-based products.^[24] Moreover, carbonyl, carboxyl, epoxy, and hydroxyl are some of the hydrophilic oxygen-containing functional groups of GO that make it easier to disperse in aqueous conditions and promote uniform distribution in the manufactured composites.^[25,26] These functional groups, nevertheless, also degrade some of the exceptional electrical and thermal conductivity of graphene.^[27] So, the reason that laser treatment induces more obvious structural changes in the GMF than the CMF is that it has more impurities and functional groups. The laser treatment will remove some of them by thermal effect and photon-induced bond breaking.

To sum up, comparing the GMF's photoresponse to that of CMF, it does not feature position sensitivity with sign change. However, its Seebeck coefficient distribution and magnitude are more than that of the CMF. Sign change aside, the laser-treated and not-treated regions can be distinguished to a good extent by the GMF as an abrupt change in photovoltage occurs. So, these two dissimilar regions might be used for featuring two distinct position-based photon sensing in small-length scales by using short GMFs.

3.2. Photon Sensing by Graded GAF

This section investigates the photovoltage response of GAF after conducting the half laser annealing treatment. The approach for GAF preparation is quite similar to what Hunter et al.^[27] adopted. The difference, however, is that multi-walled carbon nanotube (MWCNT) powder is used here to enhance the structural strength and mechanical properties of the produced GAFs.^[28,29] This is extremely important to have more robust GAFs both for experiments and practical applications. Here, MWCNTs with 15 wt.% are added to the GO paste in the GAF's synthesis procedure.

First, using deionized water and GO aqueous solution (with MWCNTs) of 30 mg ml^{-1} , a 10 mL diluted suspension with 4 mg ml^{-1} concentration is prepared. The resulting suspension is then ultrasonicated for 1 h. Next, $40\text{ }\mu\text{l}$ ethylenediamine (EDA) is added to the suspension as a nitrogen source per the synthesis procedure proposed by Deng et al.^[30] The suspension is then injected into 10-centimeter-long glass pipes with an inner diameter of 1.0 mm to form GA in the shape of microfibers. After sealing the ends of the pipes, they go through a hydrothermal reduction procedure by leaving them at 120°C for 12 h. Afterward, the GAFs are gently extracted from the pipes and soaked for 4 h in a 20 vol.% ethanol bath. Finally, GAFs with diameters of $\approx 640\text{ }\mu\text{m}$ are produced after the GO hydrogels are frozen for 8 h, and then are dried for additional 8 h. Next, nearly half of the selected

GAF is annealed under vacuum condition ($< 3\text{ mTorr}$) with a laser power of $\approx 500\text{ mW}$ for 200 s ^[27] at a laser spot size of 2 mm. The suspended sample of $2245\text{ }\mu\text{m}$ in length is shown as the inset in Figure 5c.

After irradiating the GAF at different locations with the line-shaped laser beam of 0.1 mm width and 5.5 mm length, like the GMF, the photovoltage of the GAF does not change sign when the laser moves from the laser-treated to un-treated parts (Figure 5a,b). However, its sensitivity is much higher than that of GMF and CMF. In other words, the laser power range used to get the photovoltage signal is only 1.8–13 mW, which is much lower than that of GMF. Since graphene aerogel has a much lower thermal conductivity,^[27,31,32] under the same laser heating, it will have a much higher temperature rise; therefore, the voltage change is stronger. Based on Figure 5b, an abrupt change in photovoltage is seen after $x = 1.4\text{ mm}$ where the laser-treated and un-treated regions are separated from each other. No meaningful trend is seen in t_c variation with the location on the sample. t_c has a range of 0.17 s to 1.26 s. This broad range most probably boils down to the nonuniform structure of the GAF, which will be explored more using Raman scanning. The range of t_c , however, is still showing a thermal-based origin for the photovoltage, as the t_c of the TET signal for the GAF is calculated to be 0.74 s.

Before proceeding, it is worth discussing two things here. The first one is the reason for using a range of power (not constant) for irradiating different locations of each sample. This is because the total thermal resistance from the laser heating location to the electrodes is much higher when the laser irradiates the middle point than when irradiating the sample ends. Therefore, the temperature rise will be lower if a laser of the same power irradiates the sample's ends. For having almost the same temperature rise (voltage drop), a higher laser power (heat) should be applied to the locations near the sample ends. The second one is using a distinct range of laser powers for each sample. The reason for this one is related to the distinct thermal resistance of these samples. This thermal resistance is related to the sample's thermal conductivity, length, and diameter. A sample of very high thermal resistance (e.g., GAF) will need a lower laser power. To have quite the same photoresponse ($\approx 0.1\text{--}0.3\text{ mV}$) from all three samples, we should use distinct levels of laser power. Otherwise, if we use the same laser power for all of them, either the signal will not be distinguishable for a sample, or another one will be damaged.

The Seebeck variation calculated using Equation 3 is shown in Figure 5c. Using TET, α_{eff} of the GAF is measured to be $1.2 \times 10^{-6}\text{ m}^2\text{ s}^{-1}$. The ρ_c of the GAF is considered to be $8500\text{ J m}^{-3}\text{ K}^{-1}$.^[27] So, the k of the GAF is calculated to be $0.010\text{ W m}^{-1}\text{ K}^{-1}$. The S_x change of the GAF in space, which is between $-27.2\text{ }\mu\text{V K}^{-1}$ and $+20.4\text{ }\mu\text{V K}^{-1}$, is not that much considerable, meaning that a higher level of laser heating is needed to induce more Seebeck coefficient variation. It should be noted that the laser power used here for the GAF is nearly the maximum amount before damaging the sample. Similar to the t_c , since GAF's structure is not quite uniform, the Seebeck coefficient shows strong noise and a less visible trend. After laser treatment, Raman spectroscopy scanning is conducted on the GAF to explore its structure. As shown in Figure 5d, D, G, and 2D peaks are present in the Raman signal at $\approx 1345\text{ cm}^{-1}$, $\approx 1580\text{ cm}^{-1}$, and $\approx 2682\text{ cm}^{-1}$, respectively.^[27,33,34] Moreover, no particular trend is seen in the intensity of these peaks. Based on Figure 5e,f, the I_D , I_G , and

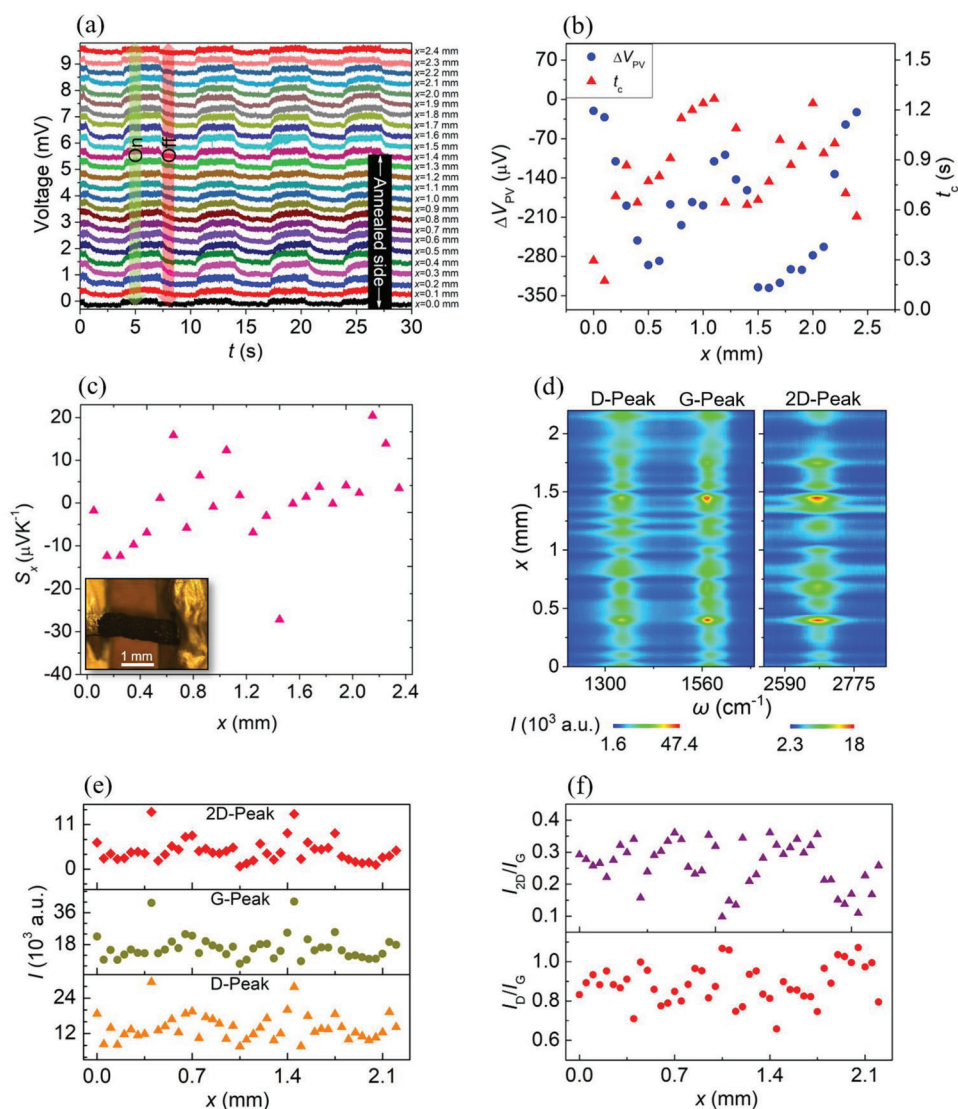


Figure 5. a) The GAF's photovoltage change with time under step laser irradiation for different locations of the sample. The “On” and “Off” status of the incident laser beam for one period is also shown. b) Photovoltage variation against locations of the GAF based on the lowest laser power (1.8 mW) used for obtaining the photoresponse. The characteristic time of the photoresponse for the GAF with location is also given. c) Local Seebeck coefficient variation of the GAF with the location. The inset is the optical image of the suspended GAF with 2.245 mm in length. d) Contour map for D, G, and 2D peaks versus Raman shift and location for the GAF. e) The D, G, and 2D peak intensities (i.e., I_D , I_G , and I_{2D}). f) D peak to G peak (I_D/I_G) and 2D peak to G peak (I_{2D}/I_G) variations for the half laser-treated GAF to show the structure variation along the sample.

(I_D/I_G) do not have a specific trend over the sample's length, indicating that the laser treatment effect is not strongly reflected in the Raman signal. Hunter et al. also reported similar findings (I_D/I_G) when comparing the reduced (laser annealed) and the original GAF with a similar laser treatment in terms of power and time used in this work.

Having analyzed the GAF, it should be considered that GAFs are too fragile and delicate compared to the CMFs and GMFs, making them less attractive for such sensing and industrial applications before doing the chemical/photoreduction.^[35,36] This is because the key component of graphene aerogel–GO nanosheets might have some oxygen-containing functional groups on flawed sites and edges, allowing for weak contact between them.

As a result of the weak interaction between neighboring GO nanosheets, GO aerogel is very fragile.^[37]

4. Conclusion

In this work, we report photon sensitivity with no external bias for three carbon-based microfibers, namely CMF, GMF, and GAF, the length of which is ≈ 2 mm. Nearly half of the sample's length was laser-treated (annealed) for a certain amount of time. The laser power used to treat the CMF and the GMF was four times bigger than that of the GAF. The microfibers were then irradiated by a line-shaped laser beam of 0.1 mm width and 5.5 mm length to probe their photoresponse to the incoming

photons versus location. Comparing the characteristic times of TET and photon sensing signals revealed the thermal effect for the photoresponse of these microfibers. During the photon sensing testing, the irradiating laser power was adjusted to have a photovoltage change of around 0.1–0.3 mV. Considering the laser power used for stimulating the samples, the GAF had the biggest photovoltage (greatest sensitivity) compared to the CMF and the GMF. Also, considering the lower laser power used to treat half of the GAF, it showed a greater Seebeck coefficient distribution, yet with no special trend along its length. No noticeable structure change was observed for the GAF after laser treatment. On the other hand, the half-laser treatment effect on the GMF's structure was noticeably captured using Raman scanning, making it capable of distinguishing the incident photon by a sharp change in the generated photovoltage magnitude. However, only the CMF was significantly position sensitive for the incoming photons with signal polarization change. A photovoltage drop was observed for the unannealed region, while a photovoltage rise in the laser-treated one. The Seebeck coefficient distribution for the CMF was the least compared to the GMF and GAF, though. Ultimately, it seems that a CMF with a higher level of laser treatment (annealing) can be a promising microfiber in practical position-sensitive photon sensing applications to take advantage of its robust structure.

Acknowledgements

This work was partially supported by the US National Science Foundation (CBET1930866 and CMMI2032464 for X. W.).

Open access funding provided by the Iowa State University Library.

Conflict of Interest

The authors declare no conflict of interest.

Data Availability Statement

The data that support the findings of this study are available from the corresponding author upon reasonable request.

Keywords

carbon microfibers, graphene aerogel fibers, graphene microfibers, position-sensitive photon sensing, Seebeck coefficient

Received: June 11, 2023

Revised: August 21, 2023

Published online:

[1] S.-H. Cheng, T.-M. Weng, M.-L. Lu, W.-C. Tan, J.-Y. Chen, Y.-F. Chen, *Sci. Rep.* **2013**, 3, 2694.

[2] K. A. Shah, M. S. Parvaiz, G. Dar, *Phys. Lett. A* **2019**, 383, 2207.

- [3] X. Cao, L. Peng, L. Liu, J. Lv, Z. Li, F. Tian, Y. Dong, X. Liu, Y. Shen, H. Sun, Y. Xu, W. Fang, C. Gao, *Carbon* **2022**, 198, 244.
- [4] M.-B. Lien, C.-H. Liu, H. Y. Chun, S. Ravishankar, H. Nien, M. Zhou, J. A. Fessler, Z. Zhong, T. B. Norris, *Nat. Photonics* **2020**, 14, 143.
- [5] S. Xu, H. Zobeiri, N. Hunter, H. Zhang, G. Eres, X. Wang, *Nano Energy* **2021**, 86, 106054.
- [6] M. Barkelid, V. Zwiller, *Nat. Photonics* **2014**, 8, 47.
- [7] H. Lee, H.-S. Kim, O. Y. Gong, J. Y. Kim, J. H. Kim, J. S. Choi, H. S. Jung, J.-Y. Park, D. H. Kim, Y.-S. Seo, T. Choi, *J. Mater. Chem. A* **2020**, 8, 10377.
- [8] T. Duan, Y. Xie, W. Xu, X. Wei, J. Cao, *ACS Appl. Electron. Mater.* **2022**, 4, 5602.
- [9] N. Aslan, *J. Mater. Sci.: Mater. Electron.* **2021**, 32, 16927.
- [10] B. Lv, Y. Liu, W. Wu, Y. Xie, J.-L. Zhu, Y. Cao, W. Ma, N. Yang, W. Chu, Y. Jia, J. Wei, J.-L. Sun, *Nat. Commun.* **2022**, 13, 1835.
- [11] X. Lu, L. Sun, P. Jiang, X. Bao, *Adv. Mater.* **2019**, 31, 1902044.
- [12] Z. Xie, J. Wang, J. T. Yeow, *ACS Appl. Nano Mater.* **2022**, 5, 7967.
- [13] J. Wang, Z. Xie, J. T. Yeow, *Mater. Res. Express* **2020**, 7, 112001.
- [14] M. Xiong, X. Shan, C. Liu, L. Yang, M. Meng, Y. Di, Z. Gan, *Applied Surface Science Advances* **2021**, 3, 100050.
- [15] M. Zhang, J. T. Yeow, *Carbon* **2020**, 156, 339.
- [16] D. Wang, A. E. L. Allca, T. F. Chung, A. V. Kildishev, Y. P. Chen, A. Boltasseva, V. M. Shalae, *Light: Sci. Appl.* **2020**, 9, 126.
- [17] J. Wang, Z. Xie, J. A. Liu, J. T. Yeow, *J. Mater. Chem. C* **2022**, 10, 15105.
- [18] B. C. St-Antoine, D. Ménard, R. Martel, *Nano Lett.* **2009**, 9, 3503.
- [19] J. Guo, X. Wang, T. Wang, *J. Appl. Phys.* **2007**, 101, 063537.
- [20] W. Qu, Y. Xue, Y. Gao, M. Rover, X. Bai, *Biomass Bioenergy* **2016**, 95, 19.
- [21] W. Qu, J. Liu, Y. Xue, X. Wang, X. Bai, *J. Appl. Polym. Sci.* **2018**, 135, 45736.
- [22] J. Liu, W. Qu, Y. Xie, B. Zhu, T. Wang, X. Bai, X. Wang, *Carbon* **2017**, 121, 35.
- [23] A. Karamati, N. Hunter, H. Lin, H. Zobeiri, S. Xu, X. Wang, *Int. J. Heat Mass Transfer* **2022**, 198, 123393.
- [24] B. Fang, D. Chang, Z. Xu, C. Gao, *Adv. Mater.* **2020**, 32, 1902664.
- [25] Y. Fadil, L. N. M. Dinh, M. O. Y. Yap, R. P. Kuchel, Y. Yao, T. Omura, U. A. Aregueta-Robles, N. Song, S. Huang, F. Jasinski, S. C. Thickett, H. Minami, V. Agarwal, P. B. Zetterlund, *ACS Appl. Mater. Interfaces* **2019**, 11, 48450.
- [26] V. Agarwal, P. B. Zetterlund, *Chem. Eng. J.* **2021**, 405, 127018.
- [27] N. Hunter, A. Karamati, Y. Xie, H. Lin, X. Wang, *ChemPhysChem* **2022**, 23, 202200417.
- [28] H. Sun, Z. Xu, C. Gao, *Adv. Mater.* **2013**, 25, 2554.
- [29] Q. Zhang, Z. Du, M. Hou, Z. Ding, X. Huang, A. Chen, Y. Ma, S. Lu, X.-Z. Tang, *Carbon* **2022**, 188, 442.
- [30] X. Deng, Q. Nie, Y. Wu, H. Fang, P. Zhang, Y. Xie, *ACS Appl. Mater. Interfaces* **2020**, 12, 26200.
- [31] Y. Xie, S. Xu, Z. Xu, H. Wu, C. Deng, X. Wang, *Carbon* **2016**, 98, 381.
- [32] Y. Xie, M. Han, R. Wang, H. Zobeiri, X. Deng, P. Zhang, X. Wang, *ACS Nano* **2019**, 13, 5385.
- [33] Y. R. Zhang, Y. Gao, Q. H. Zheng, T. T. Zhang, L. P. Qiu, S. L. Gao, X. T. Zhang, W. P. Han, Y. Z. Long, *J. Mater. Sci.: Mater. Electron.* **2022**, 33, 19947.
- [34] F. Yang, C. Liang, H. Yu, Z. Zeng, Y. M. Lam, S. Deng, J. Wang, *Adv. Sci.* **2022**, 9, 2202006.
- [35] R.-P. Ren, Z. Wang, J. Ren, Y.-K. Lv, *J. Mater. Sci.* **2019**, 54, 5918.
- [36] H. Jian, Y. Wang, W. Li, Y. Ma, W. Wang, D. Yu, *Colloids Surf. A* **2021**, 629, 127440.
- [37] Y. Shang, H. Yang, Z. Qin, S. Yin, L. Yang, M. Xu, Z. Li, Z. Jin, H. Sun, *Carbon* **2020**, 168, 169.